ADVANCED FUNCTIONAL MATERIALS
www.afm-journal.de

Graphene-Functionalized Natural Microcapsules: Modular Building Blocks for Ultrahigh Sensitivity Bioelectronic Platforms

*Lili Wang, WeiBeng Ng, Joshua A. Jackman, and Nam-Joon Cho**

Natural cellular materials with honeycomb or foam microstructures are excellent inspirations for the biomimetic design of sensitive and robust bioelectronic interfaces. Herein, the fabrication of a hierarchical, self-assembled platform that combines a natural cellular material (*Lycopodium clavatum* pollen spores) with an electrically conductive material (reduced graphene oxide, defined as rGO) for the first time is reported. The spores function as natural building blocks which are functionalized with crumpled rGO and then deposited on a silicon oxide surface, yielding a 3D architecture with electroactive properties. The hybrid material design is incorporated into a field-effect transistor device and employed in an antibody-based detection scheme in order to measure the concentration of a target protein with a limit of detection of 1×10^{-15} M, which is five orders of magnitude better than a conventional rGO-based biosensor tested in comparison. The findings in this work highlight the merit of integrating natural cellular materials with electrically conductive materials, offering a framework to develop high-sensitivity bioelectronic platforms.

1. Introduction

Natural cellular materials with honeycomb or foam microstructures are renowned for their highly efficient architectural designs that endow superior mechanical and transport properties among other functional possibilities.[1] In recent years, there has been tremendous interest in exploiting the features of cellular materials for nanotechnology applications such as energy storage, water filtration, and biosensing.[2] In nearly all cases to date, natural cellular materials have provided a design template to synthesize bioinspired material composites with compelling mechanical or electrical properties.[3] Incorporation of natural cellular materials themselves into bioelectronic platforms is very rare, and there is tremendous potential to explore how the convergence of biological and synthetic materials can improve sensing capabilities and streamline fabrication requirements.

Lycopodium clavatum spores are one of the most remarkable cellular materials in nature[2a,4] and possess a durable sporopollenin biopolymer wall that is resilient to a wide spectrum of chemical and mechanical forces.[5] Moreover, the spores are monodisperse (≈30 µm diameter), morphologically uniform, abundant in renewable supply, and biocompatible—attributes which make them attractive candidate materials over synthetic microparticles. All these factors have motivated the application of *L. clavatum* spores for materials encapsulation purposes, including drug delivery[6] and taste masking.[7] Recently, de Souza et al. demonstrated that the sporopollenin wall is an efficient support for the covalent immobilization of a lipase enzyme through generic amine chemistry that opens the door to surface functionalization.[8]

Indeed, a number of chemical strategies have been developed to endow the surfaces of materials with engineered functionalities.[4,9] One promising design has focused on the integration of materials with electrically conductive materials in order to facilitate electrical detection.[10] The self-assembly of such particles into various architectures through multiple weak interactions (e.g., hydrogen bonds, electrostatic interactions, or hydrophobic effects) has been widely reported as a means to fabricate organic optoelectronic materials.[11] Recently, many works on the design of 3D structure composite materials have also been reported, including graphene-encapsulated Co_3O_4 nanospheres,[11e] graphene-encapsulated SiO_2 nanospheres,[12] and carbon nanotube–polymer composites.[10] However, these strategies have not been extended to natural cellular materials, and addressing this gap represents an important goal

Dr. L. L. Wang, W. B. Ng, Dr. J. A. Jackman, Prof. N.-J. Cho
School of Materials Science and Engineering
Nanyang Technological University
50 Nanyang Avenue, Singapore 639798, Singapore
E-mail: njcho@ntu.edu.sg
Dr. L. L. Wang, W. B. Ng, Dr. J. A. Jackman, Prof. N.-J. Cho
Centre for Biomimetic Sensor Science
Nanyang Technological University
50 Nanyang Drive, Singapore 637553, Singapore
Prof. N.-J. Cho
School of Chemical and Biomedical Engineering
Nanyang Technological University
62 Nanyang Drive, Singapore 637459, Singapore
Dr. L. L. Wang
State Key Laboratory on Integrated Optoelectronics
College of Electronic Science and Engineering
Jilin University
Changchun 130012, P. R. China

DOI: 10.1002/adfm.201504940

toward biomimetic design of sensitive and robust bioelectronic interfaces.

Herein, we report the fabrication of a hierarchical, self-assembled platform that combines a natural cellular material (*L. clavatum* sporopollenin exine capsules, defined as LP) with an electrically conductive material (reduced graphene oxide, defined as rGO) for the first time. The spores function as natural building blocks which are functionalized with crumpled rGO and then deposited on a silicon oxide surface, yielding a 3D architecture—a *L. clavatum* sporopollenin exine capsule-reduced graphene oxide hybrid (defined as LPGH)—with electroactive properties. The LPGH design was incorporated into a field-effect transistor (FET) device and employed in an antibody-based detection scheme in order to measure the concentration of a target protein with a limit of detection (LOD) of 1×10^{-15} M, which is five orders of magnitude better than a conventional rGO-based biosensor tested in comparison. Taken together, the findings in this work highlight the potential of integrating natural cellular materials with electrically conductive materials in order to fabricate high-sensitivity bioelectronic platforms.

2. Results and Discussion

2.1. Fabrication of Electroactive LPGH Building Blocks

Figure 1a illustrates the step-by-step fabrication of an LPGH building block starting with natural *L. clavatum* spores which were previously extracted from whole spores using a well-established sequence of processing steps, including defatting, alkaline lysis, acidolysis, and serial washing followed by drying (Figure S1, Supporting Information).[13] This process yields intact sporopollenin exine capsules with an increased density of hydroxyl groups on the capsule surface,[13b,14] which facilitates the covalent attachment of (3-aminopropyl)trimethoxysilane (APTES) molecules in order to confer a positive surface charge[11e,15] as confirmed by zeta potential measurements (Figures S2 and S3, Supporting Information). The APTES coating promotes deposition of negatively charged graphene oxide (GO) through electrostatic attraction[16] and subsequent chemical reduction with hydrazine is performed in order to obtain the rGO coating. This process enables the transformation of a natural cellular material into a 3D composite structure with an electrically conductive interface.

As presented in Figure 1b,c, field emission scanning electron microscope (FESEM) images demonstrate that the surface of LP particles consists of a veined, web-like cellular architecture. After the fabrication process is complete, the LPGH building blocks exhibit similar morphological properties to the natural precursor. Figure 1d,e presents FESEM images of the LPGH composites which indicate that the cellular structure and morphology are preserved, albeit with greater interconnectivity between the web-like components and the base structure. Cross-sectional FESEM images of the LPGH composites verify the corrugated and thin (<10 nm) layer properties of the rGO shells (Figure S4, Supporting Information).

Phase-contrast images in Figure 1f,g further indicate that both the LP and LGPH composites possess a hollow morphology, as evidenced by the relatively high contrast between the shell and core. Dynamic image particle analysis (DIPA) was also employed in order to measure the morphological properties of a large number (>500) of individual microcapsules in each sample. As expected, the thin rGO coating did not affect the particle size; the average diameter of LPGH composites was ≈28.2 ± 0.2 µm versus ≈27.6 ± 0.6 µm for the LP alone (see also Figure S5 in the Supporting Information). Taken together, the findings directly support that the natural cellular materials are excellent platforms for rGO surface functionalization by a fabrication scheme that enables modular assembly.

2.2. Morphological Characterization of Graphene Coating

In order to confirm the compositional properties of the rGO coating, we then performed a detailed set of characterization experiments, as presented in **Figure 2**. LP suspended in water induce a light brown color, while LGPH composites in water exhibit a darker brown color which appears to be more similar to suspended rGO (Figure 2a). The presence of rGO in the LPGH composites was further verified by XRD analysis (Figure 2b), which showed a characteristic peak of rGO at $2\theta = 25.2°$ that is in excellent agreement with past reported values.[17]

Additionally, the XRD pattern of the LPGH composite indicates two phases of LP (◊) and rGO (♦), respectively, as compared to the XRD pattern of LP alone. The high intensity peak of rGO suggests that there is restacking of the rGO sheets which occurs during the preparation of rGO-encapsulated LP.[17b] In combination with the aforementioned FESEM characterization (cf. Figure 1d,e), multiple lines of experimental data support that rGO is present in the composite material. Raman analysis was also performed in order to verify GO reduction. Raman spectra (Figure 2f) were taken from the red arrow positions in the Raman images of Figure 2c–e, and reveal two characteristic peaks for the LPGH and rGO samples, namely the D and G bands at ≈1361 and ≈1604 cm^{-1}, respectively.[18] These chemical signatures confirm the successful reduction of rGO and the establishment of an sp^2 carbon network in the LPGH composite.[19] Moreover, the Raman spectra of LPGH display a similar D/G peak ratio to those of the rGO sheets, which supports that the sheet-like morphology of the rGO material is retained after the self-assembly procedure.[17b] Interestingly, the G band of the rGO sheets in the LPGH configuration exhibited a peak shift compared to that of the rGO sheets (Figure 2g), which indicates a strong interaction between the surface of the LP and the rGO sheets, as previously observed with metal oxide/graphene composites.[20] In addition, a peak shift in the D band was observed, possibly due to a slight difference in the degree of reduction for rGO prepared in the composite material versus in the pristine state. The strong interaction between LP and rGO in the composite structure suggests that the natural cellular material platform may not only play a structural role but also influence the electrical properties of the rGO transducing element.

2.3. Development of LPGH-Based Bioelectronic Sensing Platform

Following this line, the development of a biosensing platform was next explored based on the modular assembly of LPGH

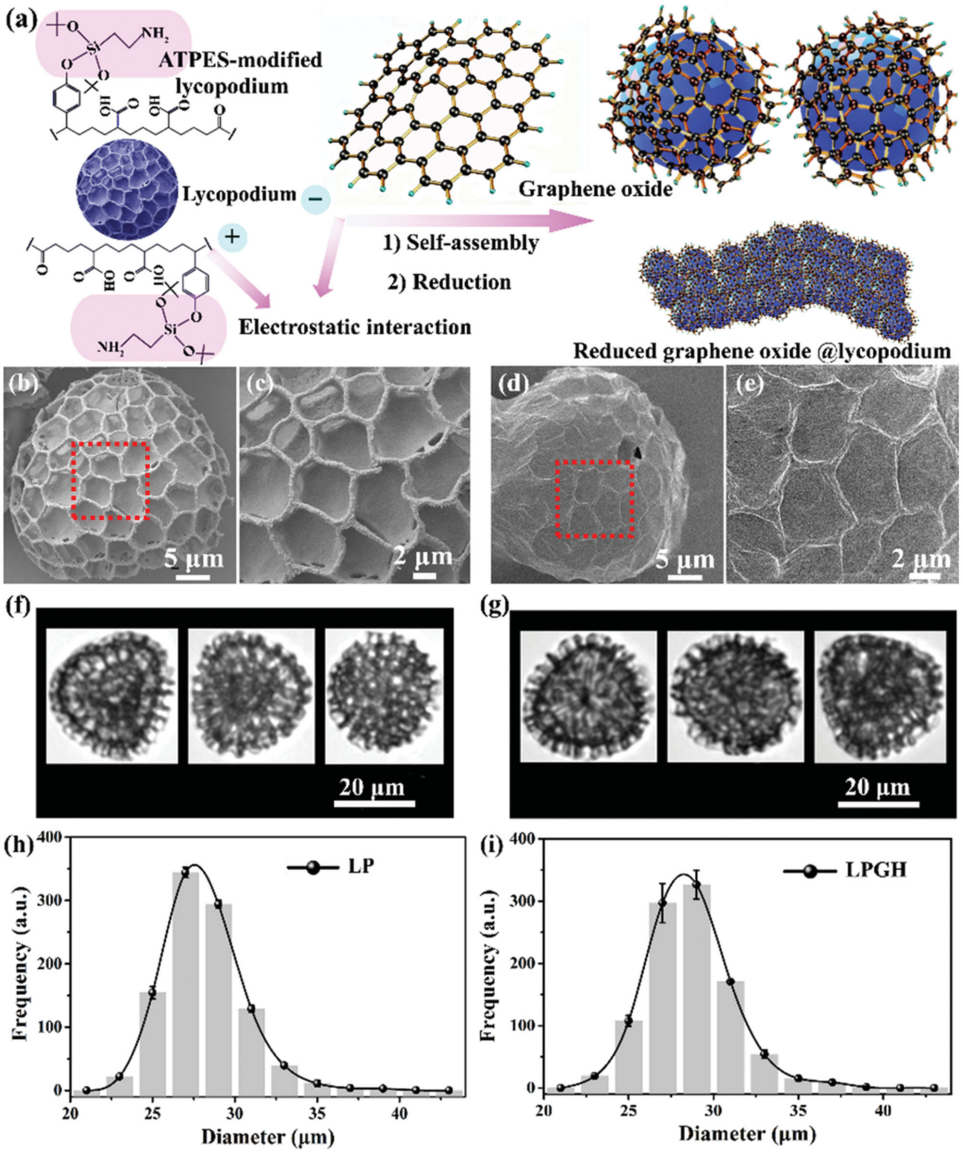

Figure 1. a) Schematic illustration of integrating a natural cellular material (LP) with an electrically conductive material (rGO). FESEM images reveal the cellular structures of b,c) LP particles and d,e) LPGH composites. DIPA images are presented for f) LP and g) LPGH. h,i) Histograms show the particle diameter before and after rGO coating, as determined by DIPA ($n = 3$ measurements).

building blocks. Key features that motivate the application of natural cellular materials such as *L. clavatum* spores in this context include natural synthesis, easy sourcing, low cost, durability, lightweight, and a high surface-to-volume ratio. Therefore, we designed a label-free measurement platform in order to detect changes in the electronic properties of LPGH when a target biomolecule attaches to the surface of the LPGH composite.[21] Biosensors of this kind primarily utilize the principle of FETs to convert biological recognition events into measurable electronic signals.[22] In a proof-of-concept demonstration, purified human C6 protein—an important component of the innate immune defense[23]—was selected as the target biomolecule.

Modular assembly of the electroactive LPGH building blocks enabled streamlined fabrication of the biosensing platform through the following steps.[24] Briefly, the positions of the source and drain electrodes were defined on a SiO_2/Si substrate by the masking film method, with a channel width of ≈100 μm (Figure S6, Supporting Information). The device fabrication was completed by deposition of metal Pt/Au electrodes with 10 nm Pt/100 nm Au on the prepatterned surface, followed by evaporation (**Figure 3**a, Step I). To introduce the LPGH sensing element into the platform, the LPGH particles were spin-coated onto the surface of the SiO_2/Si substrate (Figure 3a, Step II). In order to specifically detect C6 protein, the LPGH surface was functionalized with antihuman complement antibody (anti-C6) (Figure 3a, Step III). The antibody functionalization was conducted by first attaching APTES to the rGO surface through silane chemistry and then reacting APTES with gluteraldehyde to obtain the aldehyde-active linker which is finally conjugated

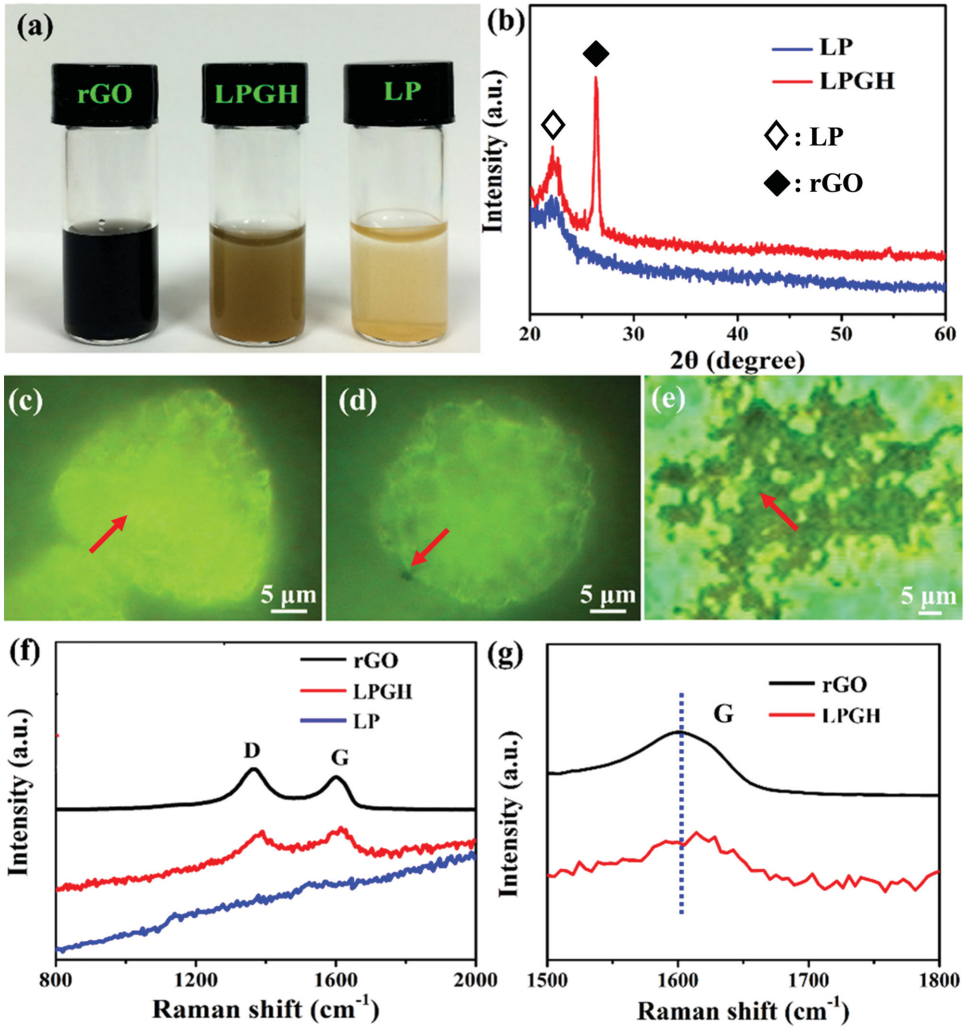

Figure 2. a) Photographs of the rGO, LPGH, and LP particles in aqueous solution. b) X-ray diffraction (XRD) patterns of LP and LPGH composites. c–e) Raman images and f) Raman spectra of LP, LPGH, and rGO sheet, respectively. Red arrows show the scan positions of the Raman spectra. g) Enlarged image of the G peak of the rGO sheet and LPGH from panel (f).

to the anti-C6 protein (Figure 3a, Step IV; see also Figure S7a, Supporting Information).[25]

Figure 3b presents an FESEM image of the channel region of the device (LPGH particles on the surface of the SiO_2/Si substrate). Once deposited on the substrate, the individual LPGH particles become adsorbed to one another and form an interconnected rGO electrical network between the source and drain electrodes. Atomic force microscopy (AFM) characterization verifies that that deposited LPGH particles are attached to one another and retain the natural morphology. (Figure S8, Supporting Information). Figure 3c–e illustrates the overall design of our measurement platform. The LPGH-based biosensing platform was confined within a small polydimethylsiloxane fence and was filled with 10×10^{-3} M phosphate-buffered saline (PBS, pH 7.4). The gate electrode, an Ag/AgCl wire, was placed in the center of the reservoir and the electrical conductance was monitored across the source and drain gold electrodes (Figure 3e). To investigate the working conditions of the LPGH biosensor in liquid conditions, its gating effect was measured. Figure 3f shows the typical relationship between the gate voltage and the source–drain current (I_{ds}) under the drain–source voltage (V_{ds}) of +0.5 V. The gating effects observed in the LPGH-based biosensor exhibited p-type behavior as well as nearly symmetric and ambipolar characteristics for the electron/hole doping region, the latter of which is similar to the characteristics of graphene.[26]

2.4. Femtomolar Detection of Target Protein

Based on this measurement configuration, we investigated the V_{ds} dependence of the I_{ds} of LPGH-based biosensors for detection of C6 protein across a wide concentration range (**Figure 4**a). In general, the electrical conductivity of the LPGH-based biosensor increased with increasing C6 protein concentration from 1×10^{-15} M to 1×10^{-9} M, and the trend in measurement responses was in good agreement with previous reports for antibody–antigen binding interactions.[25b,27]

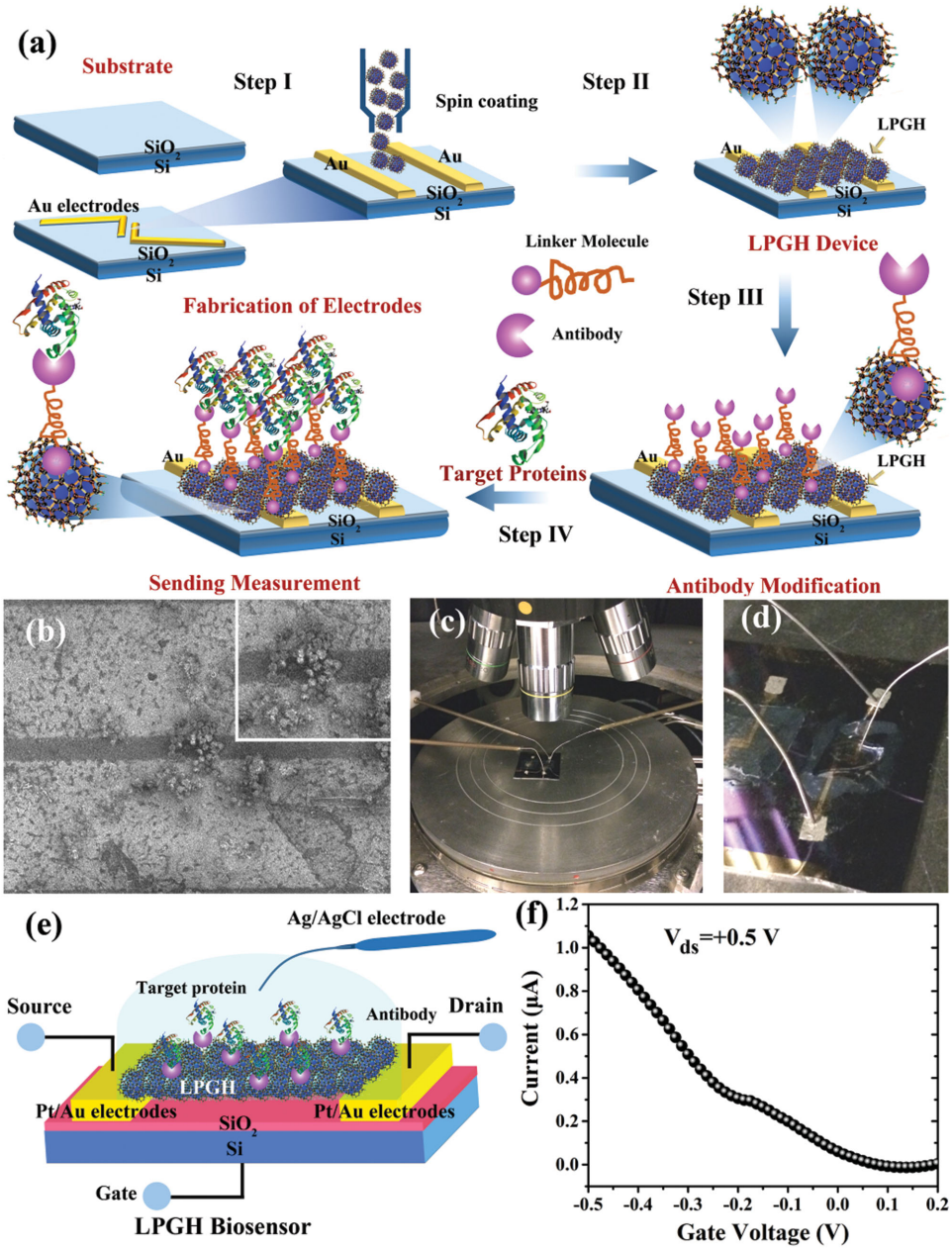

Figure 3. a) Design strategy of the LPGH-based biosensor: I) Preparation of gold electrodes on the surface of a silicon oxide/silicon (SiO_2/Si) substrate; II) Surface modification for the assembly of LPGH by the spin-coating method; III) Antibody immobilization on the surface of LPGH; IV) Electrical conductivity measurement for C6 protein detection in 10×10^{-3} M PBS. b) FESEM and (inset) magnified FESEM images of the device. c,d) Photographs of the instrument and electrodes based on LPGH. e) Schematic diagram of the process for testing the gate effect. f) Gating effect of the LPGH device at V_{ds} = +0.5 V and sweep speed of 0.05 V s^{-1}.

It was also found that the I_{ds} of the LPGH-based biosensor was slightly nonlinear, which can probably be attributed to carrier injection during the *I–V* measurement.[21b] The sensitivity of the LPGH-based biosensor was confirmed by evaluating changes in the electrical current as the C6 protein concentration was varied from 100×10^{-18} M to 100×10^{-9} M (Figure 4b). A representative sensitivity versus concentration plot indicates that addition of 100×10^{-18} M C6 protein led to no detectable response above the baseline ($I_{C6}/I_{PBS} = 1$).

However, at 1×10^{-15} M C6 concentration, a significant change in the I_{C6}/I_{PBS} ratio of the LPGH-based biosensor was detected. When the C6 concentration was further increased, the conductance change of the LPGH-based biosensor became more appreciable. As a result, the LOD of the biosensor was found to be 1×10^{-15} M C6 protein in PBS solution. The recorded measurement sensitivity was a significant advance that surpasses the known performance of conventional graphene-based thin-film-transistor biosensors.[12]

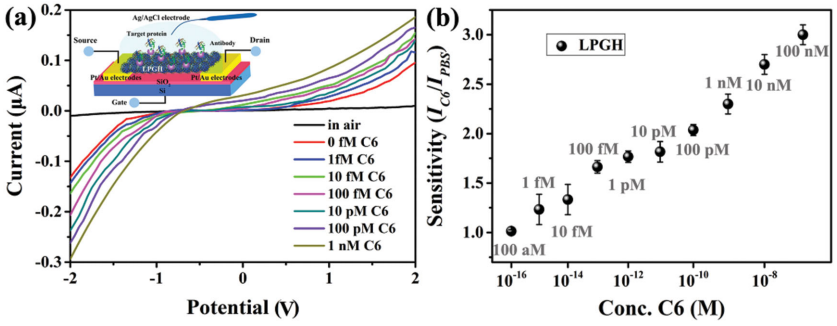

Figure 4. a) *I–V* curves of the LPGH-based biosensor responding to different concentrations of C6 antigen in PBS solution with gate voltage (V_g = 0 V). b) Sensitivity of the LPGH-based biosensor (with relative current change) as a function of the C6 concentration with V_{ds} = +0.5 V and V_g = 0 V.

In light of this finding, additional experiments were conducted using a conventional, flat rGO-based biosensor in the same measurement configuration, including equivalent antibody functionalization. It was observed that the LPGH-based biosensor had a 42% ± 2% (I_{C6}/I_{PBS}, %) increase in detection sensitivity for 10×10^{-12} M C6 protein over the flat rGO-based biosensor (Figures S7b and S9, Supporting Information). Two benefits of the natural cellular architecture appear to be prominent in enabling improved detection capabilities. First, the 3D architecture of the LPGH platform provides a greater surface area in order to detect analyte binding events.[21a] Second, the LPGH platform exhibits a significantly improved signal-to-noise ratio which enables superior detection due to more stable measurements (Figure S10, Supporting Information). Because the substrate of graphene-based devices is known to affect sensing performance along with other functionalities, it is intriguing to understand how natural cellular materials can modulate the electronic properties of graphene-based materials. We found that the surface chemistry introduced in the biosensor played a pivotal role for obtaining high sensitivity and a low LOD for biomarker proteins. More specifically, by using the synergism that occurred in these unique structures of graphene–particle hybrid materials, it was possible to achieve biomolecular detection down to the femtomolar ($\times 10^{-15}$ M) range, wherein the combination of the two materials resulted in additional surface area for analyte binding, signal amplification, and enhanced electrical conductivity.[21a]

3. Conclusion

In summary, we have developed a hierarchical, self-assembled platform that combines a natural cellular material (*L. clavatum* sporopollenin exine capsules) with an electrically conductive material (reduced graphene oxide) for the first time. The so-called LPGH platform was successfully prepared by employed strong and lightweight *L. clavatum* sporopollenin exine capsules as building blocks which were functionalized with "rGO wrappers" through a facile and convenient fabrication method. Modular assembly of the rGO-encapsulated spores led to the fabrication of a highly sensitive biosensor which exhibited a 1×10^{-15} M limit of detection for the target protein. Importantly, the LPGH platform combines the unique properties of natural cellular architectures with the sensing capabilities of graphene-based materials. Looking forward, there is significant opportunity to explore the fabrication of other graphene/natural cellular architecture composites as high-sensitivity bioelectronic platforms.

4. Experimental Section

Materials: Phosphoric acid (H_3PO_4), acetone, hydrochloric acid (HCl), potassium hydroxide solution (KOH), sodium hydroxide (NaOH), potassium chloride (KCl), sodium phosphate dibasic (Na_2HPO_4), potassium phosphate monobasic (KH_2PO_4), sodium chloride (NaCl), ethanol, APTES (98%), hydrazine (35 wt%), IPA, and toluene were purchased from Alfa Aesar. GO (>95%), glutaraldehyde solution (25%), and sodium cyanoborohydride ($NaCNBH_4$) were purchased from Sigma-Aldrich. Silicon wafers were purchased from Semiconductor Wafer Inc. Antibody-C6 and C6 protein were purchased from Complement Technology Inc. All commercially available chemicals were used as received.

Extraction of Natural L. clavatum Spores: The pollen obtained by the extraction process was defined as LP. Briefly, the process is comprised of defatting, alkaline lysis, acidolysis, and serial washing followed by drying.[1] The natural *L. clavatum* spores (100 mg) were defatted through suspension in acetone (500 mL). The defatted spores were then subjected to alkaline lysis in fresh potassium hydroxide solution (6%, w/v, 500 mL). The *L. clavatum* grains (50 g) were next suspended in phosphoric acid (H_3PO_4, 85%, v/v, 500 mL) in a 500 mL flask and mixed gently to form a homogeneous suspension. The grains were refluxed at 70 °C under gentle stirring for 30 h. Then, the *L. clavatum* grains were collected by filtration and washed extensively with hot water (5×800 mL), hot acetone (600 mL), hot 2 M hydrochloric acid (600 mL), hot 2 M sodium hydroxide (600 mL), and hot ethanol (600 mL). The LPs were dried at 60 °C for 12 h and stored in a dry cabinet at 25 °C until experiment.

Preparation of APTES-Modified L. clavatum Sporopollenin Exine Capsules (APTES-Modified LP): First, 7.5 mg of the LPs were mixed with 10 mL of toluene solution. After magnetic stirring at 30 min, 0.05 mL APTES (98%) solution was added to the solution and further stirred for 24 h in a nitrogen-rich atmosphere in order to obtain the APTES- modified LP product.

Preparation of L. clavatum Sporopollenin Exine Capsule-Reduced Graphene Oxide Hybrid (LPGH) Biomaterials: First, 10 mL of APTES-modified LP dispersion (0.75 mg mL^{-1}) was dispersed in a 20 mL aqueous solution with 0.375 mL of a 0.04 mg mL^{-1} GO sheets suspension, with moderate magnetic stirring. After 6 h, 0.5 mL hydrazine (35 wt%) was added to the solution in order to reduce the GO to rGO, and mixed with magnetic stirring for 12 h. The rGO-encapsulated LP microspheres were obtained after centrifugation and washing with water.

Fabrication of LPGH-Based Biosensor: The fabrication process of the biosensor followed the general steps outlined in the methods by Lieber et al. and Lee and co-workers.[2,3] Briefly, the LPGH materials were spin-coated (spin rate: 1000 rpm for 35 s, and then 4000 rpm for 35 s) onto the surface of the SiO_2/Si substrate with Pt/Au electrodes, and the obtained device was cleaned by oxygen plasma treatment. After that, the device was immersed into an APTES solution (1%, v/v, APTES in ethanol/water (95%/5%)) for 45 min. The device was mildly washed by isopropanol (IPA), blown dry by N_2 gas, and put in an oven at 110 °C for 10 min. Then, the device was incubated in the glutaraldehyde solution with 4×10^{-3} M $NaCNBH_4$ for 2 h, followed by washing with IPA. Finally, the device was immersed into a antibody-C6 solution (100 μg mL^{-1}) in

10×10^{-3} M PBS (pH 7.4, including 8 g L^{-1} of NaCl; 0.2 g L^{-1} of KCl; 1.44 g L^{-1} of Na_2HPO_4 and 0.24 g L^{-1} of KH_2PO_4, and 4×10^{-3} M $NaCNBH_4$ solution), followed by washing the surface with a gentle flow of 10×10^{-3} M PBS solution.

Characterization: The surface morphology and structure of all samples were taken using an FESEM 6340F (JEOL, Japan). X-ray diffraction (XRD) patterns were obtained from the X-ray diffractometer (XRD-600, Shimadzu, Japan) in the range of 20°–60° (2θ) at a scanning rate of 6° min^{-1}. The surface structure was observed by AFM (NX-Bio, Park Systems, Suwon, South Korea). The Raman spectra were acquired using a confocal Raman microscope (WITec, Ulm, Germany) with a 488 nm laser excitation, a spatial resolution of 1 μm, and an accumulation time of 3 s at each spot. Spectra for LPs and LPGH were collected. These data were representative of three independent measurements. The micromeritic properties of all samples were evaluated by DIPA. The surface charge properties of APTES-modified LP with GO were detected by zeta (ζ) potential measurements (ZetaPals Analyzer, Brookhaven Instruments, Holtsville, NY, USA, monochromatic laser: 658 nm). Electrical characterization of the fabricated LPGH-based biosensors were conducted by a Keithley 4200-SCS semiconductor characterization system with a probe station at room temperature. An Ag/AgCl wire was placed in contact with the liquid solution as a gate electrode.

Supporting Information

Supporting Information is available from the Wiley Online Library or from the author.

Acknowledgements

This work was supported by the National Research Foundation (Grant Nos. NRF-NRFF2011-01 and NRF-CRP10-2012-07) to N.J.C. L.W. is grateful for financial support from the Natural Science Foundation Committee (NSFC, Grant No. 51502110) and the Postdoctoral Science Foundation of China (Grant No. 2015M571361). The authors acknowledge Saziye Yorulmaz, Dr. Raghavendra C. Mundargi, Michael Potroz, Dr. Jeongeun Seo, Ee-Lin Tan, and Jae Park for materials and valuable discussion.

Received: November 18, 2015
Revised: December 23, 2015
Published online: February 19, 2016

[1] a) R. Lakes, *Nature* **1993**, *361*, 511; b) K. C. Cheung, N. Gershenfeld, *Science* **2013**, *341*, 1219; c) B. Sonon, B. Francois, T. J. Massart, *Comput. Mech.* **2015**, *56*, 221; d) H. S. U. Butt, P. Xue, B. Hou, *Bull. Pol. Acad. Sci. Technol. Sci.* **2015**, *63*, 181; e) X. Luo, J. Y. Xu, W. M. Li, *Funct. Mater. Lett.* **2015**, *8*, 4.

[2] a) S. C. Han, J. W. Lee, K. Kang, *Adv. Mater.* **2015**, *27*, 5506; b) U. G. K. Wegst, H. Bai, E. Saiz, A. P. Tomsia, R. O. Ritchie, *Nat. Mater.* **2015**, *14*, 23; c) L. L. Wang, T. Fei, Z. Lou, T. Zhang, *ACS Appl. Mater. Interfaces* **2011**, *3*, 4689; d) X. D. Li, W. C. Chang, Y. J. Chao, R. Z. Wang, M. Chang, *Nano Lett.* **2004**, *4*, 613; e) L. L. Wang, H. M. Dou, Z. Lou, T. Zhang, *Nanoscale* **2013**, *5*, 2686.

[3] S. Gutierrez-Gonzalez, J. Gadea, A. Rodriguez, C. Junco, V. Calderon, *Constr. Build. Mater.* **2012**, *28*, 653.

[4] C. Huang, G. Yang, Q. Ha, J. X. Meng, S. T. Wang, *Adv. Mater.* **2015**, *27*, 310.

[5] a) S. J. Archibald, S. L. Atkin, W. Bras, A. Diego-Taboada, G. Mackenzie, J. F. W. Mosselmans, S. Nikitenko, P. D. Quinn, M. F. Thomas, N. A. Young, *J. Mat. Chem. B* **2014**, *2*, 945; b) W. B. Goodwin, I. J. Gomez, Y. N. Fang, J. C. Meredith, K. H. Sandhage, *Chem. Mat.* **2013**, *25*, 4529; c) I. J. Gomez, W. B. Goodwin, D. Sabo, Z. J. Zhang, K. H. Sandhage, J. C. Meredith, *J. Mater. Chem. C* **2015**, *3*, 632.

[6] A. Diego-Taboada, L. Maillet, J. H. Banoub, M. Lorch, A. S. Rigby, A. N. Boa, S. L. Atkin, G. Mackenzie, *J. Mater. Chem. B* **2013**, *1*, 707.

[7] S. Barrier, A. S. Rigby, A. Diego-Taboada, M. J. Thomasson, G. Mackenzie, S. L. Atkin, *LWT Food Sci. Technol.* **2010**, *43*, 73.

[8] S. P. de Souza, J. Bassut, H. V. Marquez, I. I. Junior, L. S. M. Miranda, Y. K. Huang, G. Mackenzie, A. N. Boa, R. de Souza, *Catal. Sci. Technol.* **2015**, *5*, 3130.

[9] A. Hagenau, M. H. Suhre, T. R. Scheibel, *Prog. Polym. Sci.* **2014**, *39*, 1564.

[10] M. T. Byrne, Y. K. Gun'ko, *Adv. Mater.* **2010**, *22*, 1672.

[11] a) A. D. Schwab, D. E. Smith, B. Bond-Watts, D. E. Johnston, J. Hone, A. T. Johnson, J. C. de Paula, W. F. Smith, *Nano Lett.* **2004**, *4*, 1261; b) K. E. Martin, Z. C. Wang, T. Busani, R. M. Garcia, Z. Chen, Y. B. Jiang, Y. J. Song, J. L. Jacobsen, T. T. Vu, N. E. Schore, B. S. Swartzentruber, C. J. Medforth, J. A. Shelnutt, *J. Am. Chem. Soc.* **2010**, *132*, 8194; c) D. Franke, M. Vos, M. Antonietti, N. Sommerdijk, C. F. J. Faul, *Chem. Mat.* **2006**, *18*, 1839; d) Y. Y. Lin, R. Chapman, M. M. Stevens, *Adv. Funct. Mater.* **2015**, *25*, 3183; e) S. B. Yang, X. L. Feng, S. Ivanovici, K. Mullen, *Angew. Chem. Int. Ed.* **2010**, *49*, 8408.

[12] S. Myung, A. Solanki, C. Kim, J. Park, K. S. Kim, K. B. Lee, *Adv. Mater.* **2011**, *23*, 2221.

[13] a) R. C. Mundargi, M. G. Potroz, S. Park, H. Shirahama, J. H. Lee, J. Seo, N.-J. Cho, *Small* **2015**, DOI: 10.1002/smll.201500860; b) S. Barrier, *Ph.D. Thesis*, University of Hull, Hull, UK **2008**.

[14] R. B. Merrifield, *J. Am. Chem. Soc.* **1963**, *85*, 2149.

[15] S. F. Hou, S. J. Su, M. L. Kasner, P. Shah, K. Patel, C. J. Madarang, *Chem. Phys. Lett.* **2010**, *501*, 68.

[16] C. Wu, J. Maier, Y. Yu, *Adv. Funct. Mater.* **2015**, *25*, 3488.

[17] a) M. Azarang, A. Shuhaimi, R. Yousefi, M. Sookhakian, *J. Appl. Phys.* **2014**, *116*, 084307; b) A. N. Naveen, S. Selladurai, *Electrochim. Acta* **2015**, *173*, 290; c) L. Wang, X. H. Wang, X. P. Xiao, F. G. Xu, Y. J. Sun, Z. Li, *Electrochim. Acta* **2013**, *111*, 937.

[18] Y. J. Guo, S. J. Guo, J. T. Ren, Y. M. Zhai, S. J. Dong, E. K. Wang, *ACS Nano* **2010**, *4*, 4001.

[19] J. F. Rodriguez-Nieva, E. B. Barros, R. Saito, M. S. Dresselhaus, *Phys. Rev. B* **2014**, *90*, 9.

[20] a) J. F. Shen, B. Yan, M. Shi, H. W. Ma, N. Li, M. X. Ye, *J. Mater. Chem.* **2011**, *21*, 3415; b) L. Chen, B. Wei, X. T. Zhang, C. Li, *Small* **2013**, *9*, 2331.

[21] a) P. T. Yin, S. Shah, M. Chhowalla, K. B. Lee, *Chem. Rev.* **2015**, *115*, 2483; b) S. Mao, G. H. Lu, K. H. Yu, Z. Bo, J. H. Chen, *Adv. Mater.* **2010**, *22*, 3521.

[22] D. Li, M. B. Muller, S. Gilje, R. B. Kaner, G. G. Wallace, *Nat. Nanotechnol.* **2008**, *3*, 101.

[23] a) A. E. Aleshin, I. U. Schraufstatter, B. Stec, L. A. Bankston, R. C. Liddington, R. G. DiScipio, *J. Biol. Chem.* **2012**, *287*, 10210; b) A. Orren, P. C. Potter, *S. Afr. Med. J.* **2004**, *94*, 345.

[24] F. Patolsky, G. F. Zheng, C. M. Lieber, *Nat. Protoc.* **2006**, *1*, 1711.

[25] a) O. S. Kwon, S. J. Park, J. Y. Hong, A. R. Han, J. S. Lee, J. S. Lee, J. H. Oh, J. Jang, *ACS Nano* **2012**, *6*, 1486; b) J. H. An, S. J. Park, O. S. Kwon, J. Bae, J. Jang, *ACS Nano* **2013**, *7*, 10563.

[26] J. S. Bunch, A. M. van der Zande, S. S. Verbridge, I. W. Frank, D. M. Tanenbaum, J. M. Parpia, H. G. Craighead, P. L. McEuen, *Science* **2007**, *315*, 490.

[27] X. X. Duan, N. K. Rajan, D. A. Routenberg, J. Huskens, M. A. Reed, *ACS Nano* **2013**, *7*, 4014.